Chapter 3

Chapter 3.Chemometric-based analysis of myco-metabolite of bioactive enriched fraction of *Pleurotus osteratus* and its correlation with *in-vitro* cytotoxic activity

3.1. Background

In the preceding chapter, DCM: Et crude extract showed significantly higher cytotoxic potential in contrast to hydroalcoholic crude extract. Among the species studied, *P. osteratus* and *P. florida* had exceptionally good cytotoxic potential. In continuation, in the present chapter, bio-assay guided fractionation of DCM: Et crude extracts of *P. osteratus* (PO1) was carried out and further explored the *in-vitro* cytotoxic activity of PO1 and its potent fractions against a panel of human cancerous cell lines. Polyphenols and ergosterol were the known lower molecule weight myco-metabolite attributing to anti-cancer activities; hence their quantitative profiling in the crude extract and its potent fractions were conducted using liquid chromatography with tandem mass spectrometry (LC-MS/MS). Moreover, untargeted myco-metabolite profiling was also performed using liquid chromatography–hybrid quadrupole time-of-flight mass spectrometry (LC–QTOF/MS), to identify novel biomarkers. Unsupervised chemometric model: principal component analysis (PCA) and hierarchical cluster analysis (HCA) and supervised chemometric model: partial least square (PLS) were applied to discriminate and distinguish potent extract and fraction based on myco-metabolite contributing to the bioactivitie

3.2. Objectives

- Bio-assay guided fractionation of DCM: Et crude extract of *P. osteratus* (PO1).
- Evaluation of *in-vitro* cytotoxic activity of PO1 and its potent fraction against a panel of human cancer cell lines.
- LC-MS/MS polyphenols and ergosterol-based targeted quantitative profiling of PO1 and its potent fraction.
- LC-QTOF/MS-based untargeted myco-metabolite profiling of PO1 and its potent fraction.
- Unsupervised (PCA and HCA) and supervised (PLS) chemometric analysis of PO1 and its potent fraction.

3.3. Experimental work

3.3.1. Material, Chemicals, and Reagents

P. osteratus mushroom was procured from Sigma bioengineering and technologies, Varanasi. All the cell lines were procured from NCI-Bethesda, USA. Authentic standards of p-coumaric acid (COUA), apigenin (API), kaempferol (KAM), luteolin (LUT), naringenin (NA), quercetin (QE) and ergosterol (E) were procured from Sigma-Aldrich, Mumbai, India. Chlorogenic acid (CA) and protocatechuic acid (PA) were purchased from HWI Analytik, GmbH, Germany. All other chemicals used were of analytical grade.

3.3.2. Authentication

3.3.2.1. Molecular characterization

Genomic DNA was extracted from pure culture and dried mushroom using Macherey-Nagel NucleoSpin Plant II Kit (Macherey-Nagel, Duren, Germany), following the manufacture's protocol (Macherey-Nagel, 2014). Agarose gel electrophoresis was

conducted for DNA quality check. Using the primers ITS-1F (5′-TCCGTAGGTGAACCTGCGG -3′) and ITS-4R (5′- TCCTCCGCTTATTGATATGC -3′), double-stranded DNAs from the ITS region were amplified by polymerase chain reaction (PCR). Amplicons of fungal strain were obtained by using the following mix reaction: 10 µL Phire Hot Start II PCR Master Mix kit (Thermo Fisher Scientific, Massachusetts, United States), 0.5 µL forward primer, 0.5 µL reverse primer, genomic DNA template 2 µL, and sterile water to a final volume of 20 µL. PCR stages include initial denaturation stage at 98°C for 30 sec, followed by 40 cycles of denaturation (98°C, 5 sec), annealing (58°C, 10 sec), and extension (72°C, 15 sec), and a final extension for 60 sec at 72°C along with a final hold at 4°C. PCR product quality was visualized by agarose gel electrophoresis. Further, PCR product was treated with ExoSAP-IT (GE Healthcare, Illinois, United States) for removing unwanted primers dNTPs from a PCR product, as per manufacture protocol (Amershambiosciences, 2000). The sequencing reaction was done in a PCR thermal cycler (GeneAmp PCR System 9700, Applied Biosystems, Massachusetts, United States) using the BigDye Terminator v3.1 Cycle Sequencing Kit (Applied Biosystems, Massachusetts, United States), following manufactures protocol (Biosystems, 2002). The sequence quality was checked using Sequence Scanner Software v 1.0 (Applied Biosystems, Massachusetts, United States). Sequence alignment and required editing of the obtained sequences were carried out using Geneious Pro v 5.1. The sequence homology analysis was executed using the basic local alignment search tool (BLAST) search in GenBank (NCBI).

3.3.2.2. Taxonomical characterization

Descriptive characteristics of mushrooms were studied macroscopically by observing pileus color and its dimension, stipe color and its dimension, and gills features. Microscopic characteristics were observed by free hand sections of dried basidiocarps

and mounting in 3% potassium hydroxide, followed by staining with 1% aqueous congo red. Line drawing of microscopic characteristics was drawn with the aid of camera lucida, and measurements were measured for each character for the description of the average dimension.

3.3.3. Bioassay guided fractionation

Based on preliminary bio-activity screening of different crude extracts of *Pleurotus* mushroom, DCM: Et crude extract of *P. osteratus* (PO1) (72 g) was further fractionated into different solvents of increasing polarities such as hexane (HFPO1) (5 g), ethyl acetate (EFPO1) (4.5 g), butanol (BFPO1) (32.4 g), and aqueous (AFPO1) (18 g) and were screened for cytotoxicity potential.

3.3.4. *In-vitro* cytotoxic activity

A similar procedure was repeated for *in-vitro* cytotoxic activity, as described in Chapter 2 (Section 2.3.5.), for screening different fractionate of PO1 against MDA-MB-231, and human lung cancer cell line (A549). The cell lines were treated with different concentrations - 1000 µg/mL, 500 µg/mL, 250 µg/mL, 125 µg/mL, 62.5 µg/mL, 31.25 µg/mL, and 15.625 µg/mL for 48 hours.

PO1 and the most potent fractionate were further screened against panels of human cancer cell lines: human breast cancer cell line (MDA-MB-231, Hs578t, and MCF-7), human blood cancer cell line (HL-60 and Molt-4), human lung cancer cell line (A549 and NCI-H 322), human pancreatic cancer cell line (Panc-1 and MiaPaCa-2) and human oral cancer cell line (SCC-9 and FaDu), with different concentrations - 1000 µg/mL, 500 µg/mL, 250 µg/mL, 125 µg/mL, 62.5 µg/mL, 31.25 µg/mL and 15.625 µg/mL for 24 hours.

3.3.5. LC-MS/MS-based quantitative profiling of phenolic acids, flavonoids, and ergosterol

The quantitative estimation of phenolic acids, flavonoids, and ergosterol were performed using Agilent 6470 triple-quadrupole mass spectrometer coupled with 1260 Infinity II Prime LC (Agilent, California, United States). The separation was carried out on Pursuit 3 PFP (3 µm, 150 X 2 mm) column (Agilent, California, United States) at the flow rate of 0.43 mL/min with sample volume 5 µL, using the gradient mobile phase: 0.1% aqueous formic acid containing 5 mM ammonium formate (A) and 0.1% formic acid in methanol (B). The gradient program for pump B was as follows: 0.0–0.5 min, 2.0%; 0.5-5.0 min, 50%; 5.0–20.0 min, 98%; 20.0–25.0 min, 2%. The column temperature was set at 40°C. The mass spectra were acquired in both positive and negative modes using jet stream electrospray ionization (ESI), and quantification of all analytes was carried out in multiple reaction monitoring (MRM) mode. The optimized MRM parameters for all standards are summarized in Table 3.1. The mass spectrometer was operated under the following conditions: nebulizer gas pressure 40 bar, nebulizer gas flow 10 L/min, gas temperature 300°C; sheath gas heater temperature 250°C, sheath gas flow 11 L/min, capillary voltage 4500 V and charging voltage 500 V. MassHunter workstation software (Agilent, California, United States) was used to control the instruments as well as acquire and process the data.

Table 3.1. Optimized MRM conditions for phenolic acids, flavonoids, and ergosterol estimation.

Compound	Precursor ion	Product ion	Retention time (min)	Collision energy	Cell accelerator voltage	Polarity
API	269	151	9.474	28	5	Negative
API	269	117.1	9.474	40	5	Negative
CA	355.1	163	5.367	12	5	Positive
CA	355.1	145	5.367	36	5	Positive
EA	303	257	8.419	32	5	Positive
EA	303	201	8.419	44	5	Positive

Table 3.1. Continued

Compound	Precursor ion	Product ion	Retention time (min)	Collision energy	Cell accelerator voltage	Polarity
EA	301	284	8.419	36	5	Negative
ERG	379	69	18.578	30	5	Positive
KAM	287	153	8.800	40	5	Positive
KAM	287	69.1	8.800	50	5	Positive
LUT	285	151	8.810	28	5	Negative
LUT	285	133	8.810	40	5	Negative
NA	271	151	8.450	16	5	Negative
NA	271	119.1	8.450	28	5	Negative
COUA	165.1	147	6.070	12	5	Positive
COUA	165.1	91	6.070	28	5	Positive
PA	153.1	109	3.110	4	5	Negative
PA	153.1	108	3.110	4	5	Negative
QE	301	179	8.470	20	5	Negative
QE	301	151	8.470	24	5	Negative

3.3.6. LC-QTOF/MS-based untargeted myco-metabolite profiling

The untargeted myco-metabolite profiling was carried out by Agilent 6550 iFunnel Q-TOF coupled with 1290 Infinity LC system (Agilent, California, United States). The gradient elution was performed on ZORBX Eclipse Plus C18 (5 µm, 150 X 2.1 mm) column (Agilent, California, United States) at the flow rate of 0.3 mL/min with sample volume 5 µL, using the mobile phase: 0.1% aqueous formic acid (A) and acetonitrile containing 0.1% formic acid (B) for 30 min. The gradient program for pump B was as follows: 0.0 - 1.0 min, 5%; 1.0 - 20.0 min, 100%; 20.0 - 25.0 min, 100%; 26.0 - 30.0 min, 5%. Full scan mode was operated in both positive and negative mode using jet stream electrospray ionization from tune mass range 100 to 3200 m/z. The mass analysis was executed with the following parameter: ion source dual AJS ESI, MS/MS scan rate: 1 spectrum per second, capillary voltage 3500 V, fragmentor voltage 175 V, and skimmer potential 65 V. The stream parameters were: gas temperature 300°C, gas flow 11 L/min, and nebulizer gas pressure 40 bar. Data acquisition and processing were commanded by Agilent MassHunster software (Agilent, California, United States).

3.3.7. Chemometric analysis

An exploratory analysis of myco-metabolite from LC-QTOF/MS-based untargeted profiling, in terms of relative abundance of the base peak of identified metabolites was carried out using an unsupervised descriptive model: PCA, and HCA. Such analysis displays the myco-metabolite difference among crude extract and fraction under study. Furthermore, a supervised predictive model (PLS) was performed to highlight the correlation between the X variable (myco-metabolite from untargeted profiling) and the Y variable (*in-vitro* cytotoxic activity). Permutation analysis and variable importance in projections (VIP) was accessed to further cross-validate and significance of the PLS model. Data were analyzed using SIMCA software (Umetrics, Umeå, Sweden).

3.3.8. Headspace Gas Chromatography (GC-HS) based solvent residual analysis

For analysis of hexane, and ethyl acetate solvent residual in HFPO1, and EFPO1 samples, the GC-HS based analysis was performed by Institute of Pesticide Formulation Technology (IPFT), Gurgaon. The instrumentation includes GC-HS (7890, Agilent, USA) equipped with a head space injector, CombiPAL automatic headspace sampler, capillary column (HP-5, 30 m length, 0.25 µm film thickness and 0.28 mm id), temperature- controlled oven, capillary flow technology (CFT), and a flame ionization detector (FID).

3.4. Result and discussion

3.4.1. Authentication

3.4.1.1. Molecular characterization

For molecular characterization, DNA fingerprinting was performed for pure culture and fresh mushroom of *P. osteratus* to verify the taxonomic identity for assuring its quality. The ITS region of pure culture and fresh mushroom of *P. osteratus* were sequenced using universal primers, and BLAST analysis was conducted for the determination of sequence

homology against authenticate published ITS sequences in GenBank. The chromatogram of ITS query sequence of pure culture and fresh mushroom are attached in *Appendix* (Figure A1, and Figure A2, respectively).

The BLAST analysis of ITS sequenced of pure culture and fresh mushroom showed a percentage identity of 91.99% and 100% to *Pleurotus ostreatus* TENN 53662 ITS region (Accession: NR_163515.1), respectively. The detailed inference of BLAST analysis of ITS sequenced region of pure culture and fresh mushroom is shown in Table 3.2.

Table 3.2. Inference of BLAST analysis.

Parameters of BLAST analysis	**Results**		**Inference**
	Pure culture	**Fresh mushroom**	
No. of hit	2	3	
Description of best match species	*Pleurotus* ostreatus TENN 53662 ITS region; from TYPE material	*Pleurotus* ostreatus TENN 53662 ITS region; from TYPE material	
Accession	NR_163515.1	NR_163515.1	
E- value	2e-133	1e-36	E- value provides information about the probability that a given sequence match is purely by chance. The lower the E- value, less likely that a match is by random chance, thus more significant the match. If E <1e-50, it indicates extremely high confidence that the database match is a result of homologous relationships.
Percentage identity	91.99%	100%	Higher the percentage, the more the match is related.

The graphical summary of BLAST analysis of pure culture and fresh mushroom is represented in Figure 3.1.a and 3.1.b, respectively. The colored horizontal bars allow quick identification of the number of database hits and the degrees of similarity of the hits. The color code corresponds to the ranking of similarities of the sequence hits (Red: more related, green and blue: moderately related, and black: unrelated). The length of bars represents spans of sequence alignments relative to the query sequence. As shown in Figure 3.1.a-b, the first red line representing *P. osteratus* is more related match with better alignment of the subject sequence to query sequence.

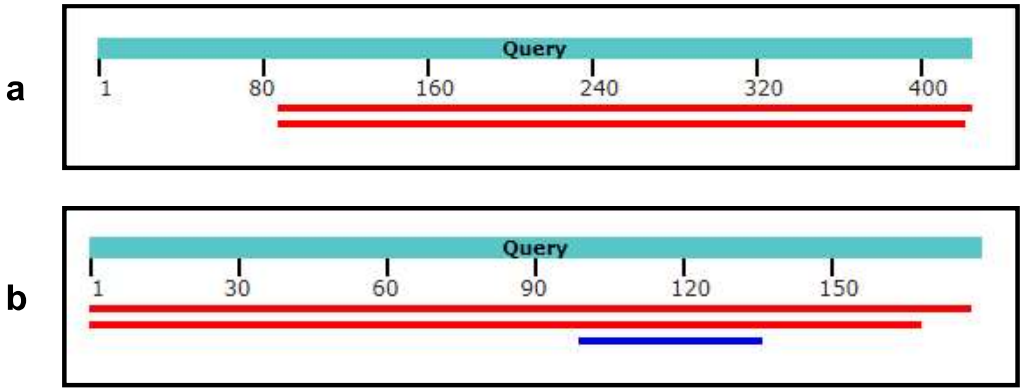

Figure 3.1. Graphical summary of BLAST analysis (a) pure culture, and (b) fresh mushroom of *P. osteratus*.

3.4.1.2. Taxonomical characterization

The macroscopic and microscopic features of *P.osteratus* are detailed below:

Macroscopic features:

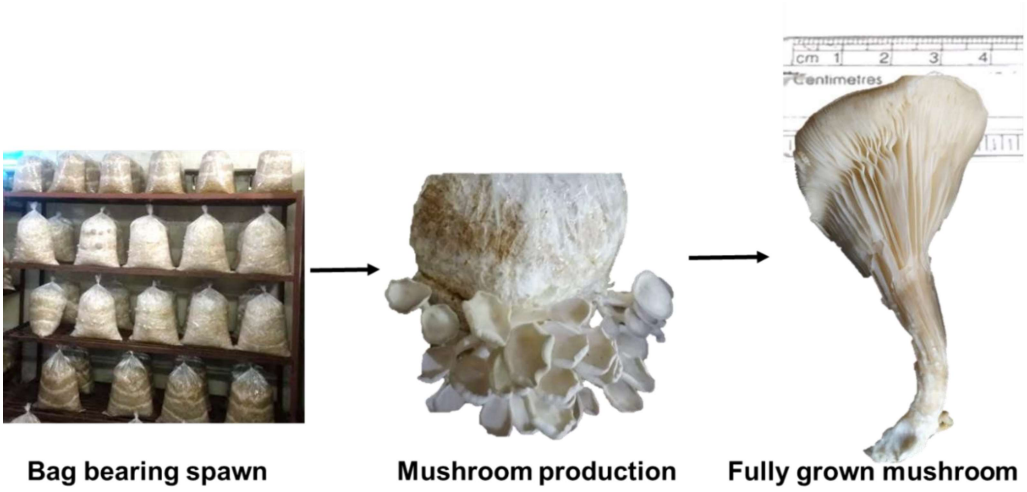

Figure 3.2. Morphological growth of *P.osteratus*.

The Macroscopic characteristics of *P. osteratus* with pictorial view (Figure 3.2.) are:

Context: White to grey-white, fleshy, radially fibrous, fungoid odour and a mild taste

Pileus: 2-4 cm, conchate shape or oyster shape, smooth texture with undulating margin

Gills: Decurrent and crowded

Stipe: Usually absent but if present, 0.2-0.5 cm, eccentric and laterally attached.

Microscopic features:

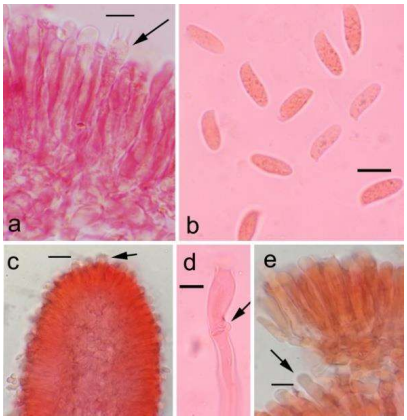

Figure 3.3. Microscopic features of *P. osteratus* (a) Basidia (b) Basidiospores (c) Cheilocystidia (d) Generative hyphae showing clamp connections, and (e) Pleurocystidia scale bar (a-e) = 10µm.

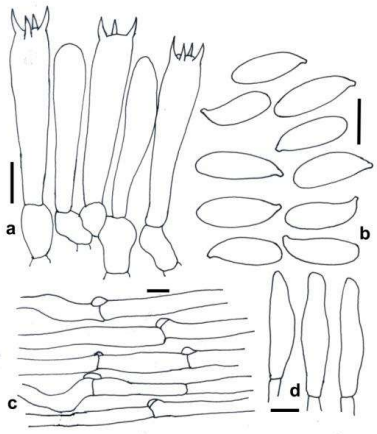

Figure 3.4. Line drawings of microscopic features of *P.osteratus* (a) Basidia (b) Basidiospores (c) Generative hyphae showing clamp connections, and (d) Pleurocystidia scale bar (a-d) = 10µm.

Basidiospores (10-)12-14(-15) × (3-)4-5(-5), a_v L = 11.8 µm, a_v W =4.2µm, a_v Q = 2.9 µm, cylindrical, in amyloid, smooth, thin-walled; Basidia 26.0 - 42.0 × 6.0 - 8.0 µm, cylindrical, hyaline, thin-walled, smooth, 2 - 4 spored; Sterigmata 4.0 - 6.0 µm long, 2 - 4 in number; Pleurocystidia 23.0 - 45.0 × 4.0 - 5.5 µm, cylindrical with capitate apices, hyaline, thin-walled, smooth; Cheilocystidia 11.0 - 23.0 × 4.5 - 6.5 µm, clavate to subclavate, hyaline, thin-walled, smooth, abundant; Lamellar tramamonomitic composed of hyphae 4.0 - 11.0 µm wide, septate with prominent clamp connections, hyaline, smooth, thin-walled, branched. The stained image and line drawing are portrait in Figure 3.3. and Figure 3.4., respectively. Based on the macroscopic and microscopic characterization of studied mushrooms, the resultant features resemble *P. osteratus*.

3.4.2. *In-vitro* cytotoxic activity

The *in-vitro* cytotoxic activity of PO1 and its fractions against MDA-MB-231 and A549 cell line are shown in Figure 3.5.a and Figure 3.5.b, respectively. Based on the IC_{50} data, HFPO1, and EFPO1 fractions showed significantly higher cytotoxic potential against MDA-MB-231, and A549 cell line, as compared to BFPO1, and AFPO1. Amongst the

sample studied, PO1, HFPO1, and EFPO1 exert potent cytotoxic potential against a given cell line.

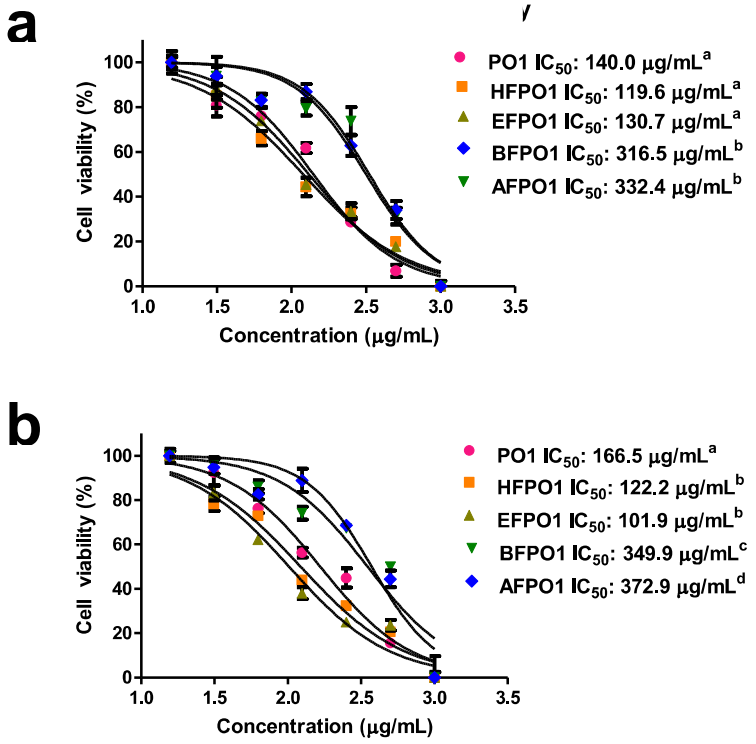

Figure 3.5. *In-vitro* cytotoxic activity of PO1 and its fraction against MDA-MB-231 and A549. Non-linear regression analysis was performed for the determination of IC_{50}. Values are expressed as mean ± standard deviation (SD) of three parallel measurements. One-way ANOVA was performed, followed by a turkey's multiple comparison test using Graph pad prism 5.0. Different letters (a, b, c, and d) represent a significant difference at ($p < 0.05$), and the same letter indicates the absence of a significant difference between the results.

The potent crude extract and the fraction (PO1, HFPO1, and EFPO1) were subjected to *in-vitro* cytotoxic activity against eleven different human cancer cell lines: MDA-MB-231, Hs578t, MCF, HL-60, Molt-4, A549, NCI-H 322, Panc-1, MiaPaCa-2, SCC-9, and FaDu. Among the panel of human cancer cell line under study, the given crude extract and its fraction were strongly cytotoxic against the human blood cancer cell line (HL-60 and Molt-4 with IC_{50} <100 µg/mL), moderately cytotoxic against the human breast cancer cell line (MDAMB-231, Hs578t, and MCF-7), human lung cancer cell line (A549

and NCI-H 322), and human oral cancer cell line (SCC-9 and FaDu) with IC_{50} range 110 µg/mL-300 µg/mL and weakly cytotoxic (IC_{50} >300 µg/mL) against human pancreatic cancer cell line (Panc-1 and MiaPaCa-2). The *in-vitro* cytotoxic activity (IC_{50}) of PO1, HFPO1, and EFPO1, represented in the form of a heat map against different cancer cell lines, is shown in Figure 3.6. From the result shown, HFPO1 fraction showed exceptionally strong cytotoxic potential against the human blood cancer cell line, human breast cancer cell line, and human oral cancer cell line. Comparatively, on the ground of the above-mentioned study result, the HFPO1 fraction stood out in cytotoxicity, followed by EFPO1 and PO1.

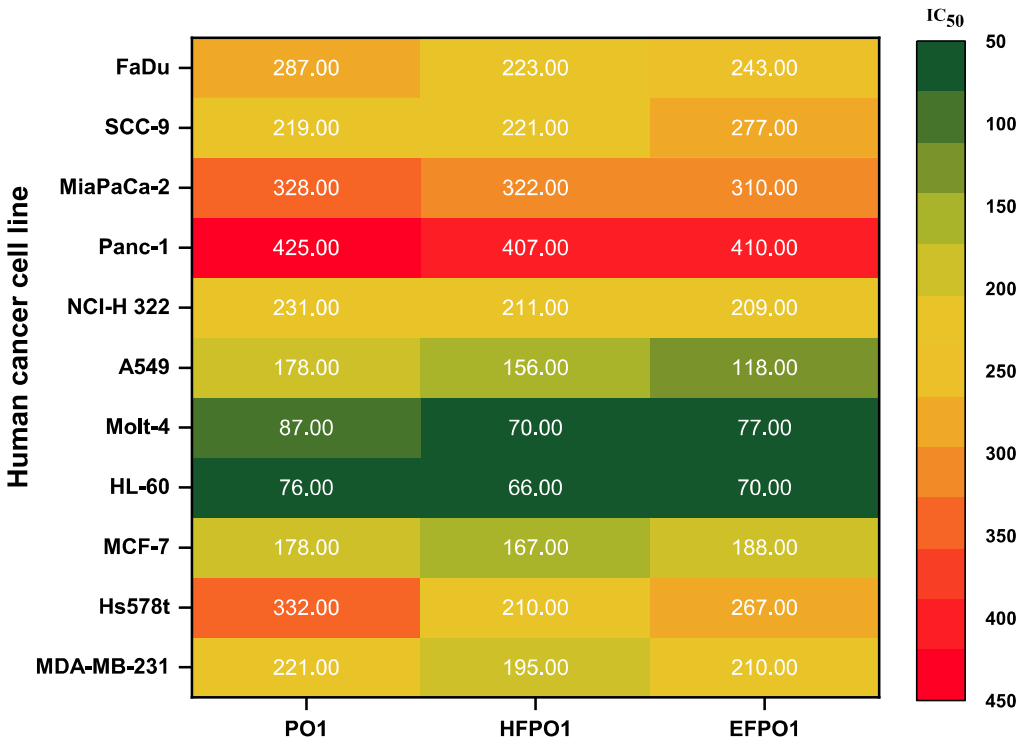

Figure 3.6. Heat-map representation (IC_{50}) of PO1, HFPO1, and EFPO1 fraction against the panel of cancer cell lines.

3.4.3. LC-MS/MS-based quantitative profiling of phenolic acids, flavonoids, and ergosterol

Hu Q *et al.* (2018) reported the anti-proliferative activity of polyphenol-rich extract of *P. eryngii* against colon cancer cells. UHPLC-MS/MS-based identified polyphenols, claiming cytotoxic activity of *P. eryngii* were gallic acid, syringic acid, ellagic acid, catechin, and methyl gallate. In the same direction, Menaga and co-worker (2021) isolated 3-methoxy 4-hydroxy benzoic acid, a phenolic acid, from *P. osteratus*, and studied its cytotoxicity against lung cancer cell lines. Beyond polyphenols, as per Krishnamoorthy (2016), ergosterol, a sterol derivative with a total content of 48 % by HPLC marker-based quantification, showed anti-cancer activity against DMBA-induced breast cancer in rats. Likewise, Finimundy *et al.* (2018a) studied the cytotoxic activity of *P. sajor-caju* against colon cancer cell line, and as per the GC-MS report, ergosterol was one of the main bioactive molecules. In continuation, LC-MS/MS polyphenol and ergosterol-based targeted profiling and quantification of *P.osteratus* was performed.

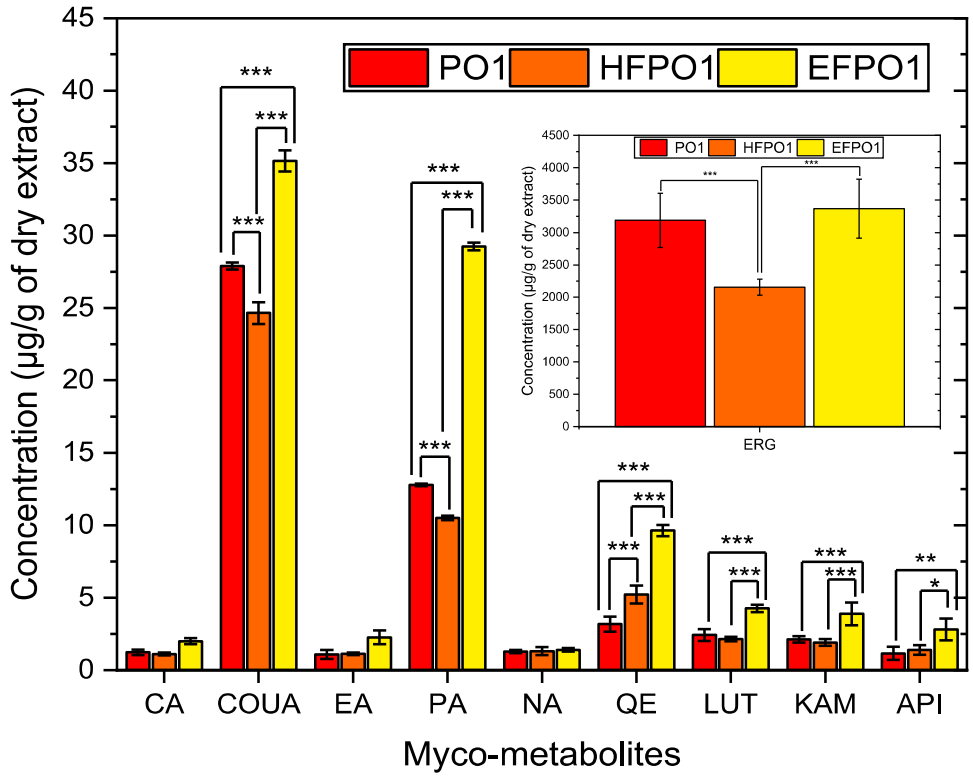

Figure 3.7. Polyphenolic content of PO1, HFPO1, and EFPO1, with inset figure showing ergosterol content of PO1, HFPO1, and EFPO1. The value are expressed as mean ± standard deviation (SD). One-way ANOVA was performed followed by the turkey's multiple comparison test using Graph pad prism 5.0. *** Significance difference ($p < 0.001$), ** significance difference ($p < 0.05$), and * significance difference ($p < 0.01$).

In this study, we identified and estimated four phenolic acids (chlorogenic acid, p-coumaric acid, protocatechuic acid, and elllagic acid), five flavonoids (naringenin, quercitin, luteolin, kaempferol, and apigenin), and ergosterol in PO1 and its HFPO1 and EFPO1 fractions. The phenolic acids, flavonoids, and ergosterol levels in PO1 and its HFPO1 and EFPO1 fractions are summarized in Figure 3.7. Among all the 9 phenolic compounds detected, there was a significant difference in the phenolic compound such as COUA, PA, and QE among all the samples ($p < 0.001$). Whereas significant difference was observed in LUT, KAM, and API content between PO1 and HFPO1, and HFPO1 and EFPO1 ($p < 0.05$) and ($p < 0.01$). Conversely, a significant difference was observed in the amount of ergosterol between PO1 and HFPO1, and HFPO1 and EFPO1 ($p <$

0.001) as shown in the inset figure of Figure 3.7. As per LC-MS/MS-based quantification of polyphenolic and ergosterol content, EFPO1 was significantly rich in ergosterol and polyphenolic content. The most abundant polyphenols in EFPO1 were p-coumaric acid, protocatechuic acid, luteolin, kaempferol, quercetin, and apigenin.

3.4.4. LC-QTOF/MS-based untargeted myco-metabolite profiling

Natural products are known for their complex metabolite networking, thus efficient elution and identification of metabolite are considered pivotal steps for claiming their therapeutic intervention. Despite being significantly rich in polyphenol and ergosterol content, EFPO1 showed moderate cytotoxicity. With the aim to explore unidentified myco-metabolite responsible for bio-activity, PO1, HFPO1, and EFPO1 were subjected to untargeted myco-metabolite screening by LC-QTOF/MS. Chromatograms of PO1, HFPO1, and EFPO1 are shown in Figure 3.8.

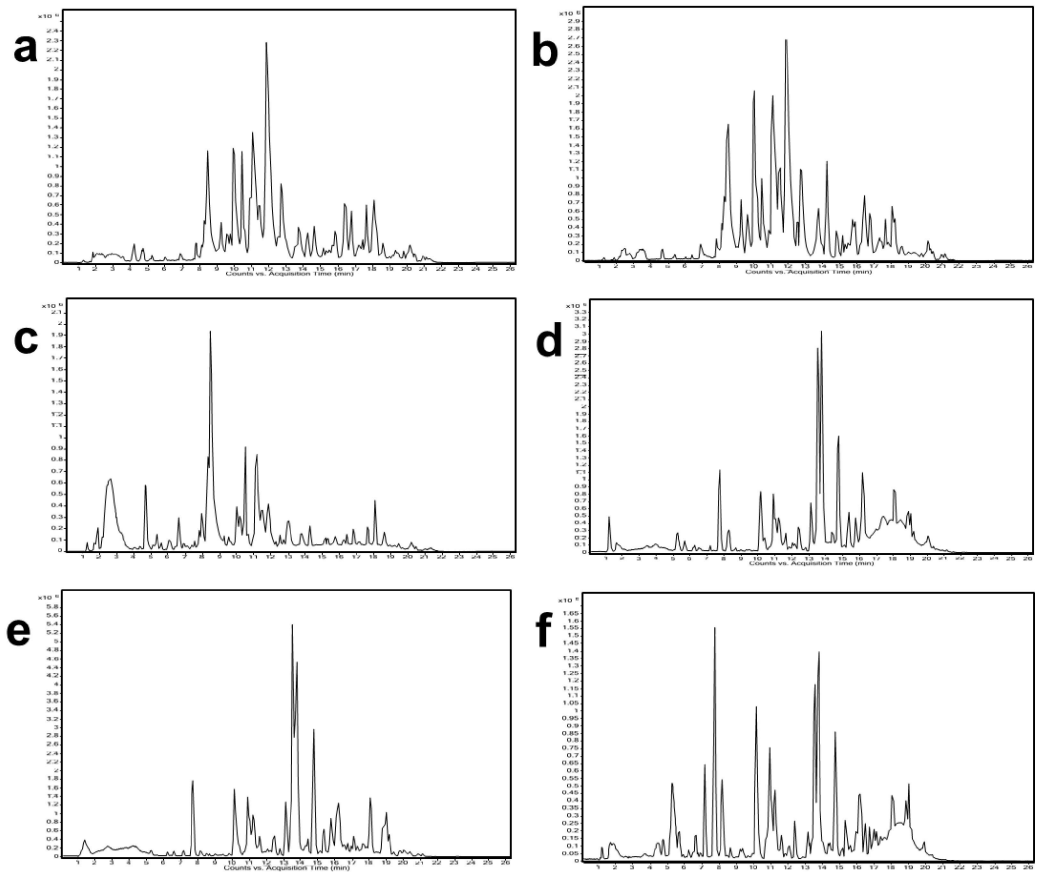

Figure 3.8. Chromatogram of PO1, HFPO1, and EFPO1 (a) (b), and (c) Chromatogram of PO1, HFPO1, and EFPO1 in positive mode, respectively and (d) (e), and (f) Chromatogram of PO1, HFPO1, and EFPO1 in negative mode, respectively.

Mass spectra of individual myco-metabolite identified are shown in Figure 3.9. A total of 20 myco-metabolites were tentatively characterized and identified by comparing retention times, molecular formula, the molecular mass of the parental ion, and MS/MS fragmentation pattern with the database (mass error < 5 ppm). Tentative identification of myco-metabolites along with their mass details, are listed in Table 3.3. Of 20 myco-metabolite identified, cholestane steroids (asterosterol and cholest-5-ene), triterpenoids (ophiobolin F, betulin, (13R,14R)-7-labdene-13,14,15-triol and (3b,6b,8a,12a)-8,12-epoxy-7(11)-eremophilene-6,8,12-trimethoxy-3-ol), fatty alcohol (linoleoyl ethanolamide, and avocadyne 4-acetate), steroidal alkaloid (16,28-Secosolanidan-23-ol,3-amino-16,23-epoxy-, (3beta,5alpha,16alpha,22alpha,23beta,25beta)-), and

polyketides (myxalamid B, and momordol) class of myco-metabolites were present in appreciable abundance in HFPO1.

Contrary, EFPO1 showed a appreciable abundance of the alkaloid (senecionine, cephaeline, and acremoauxin A), and PO1 exhibited a moderate abundance of steroids, terpenoid and alkaloid.

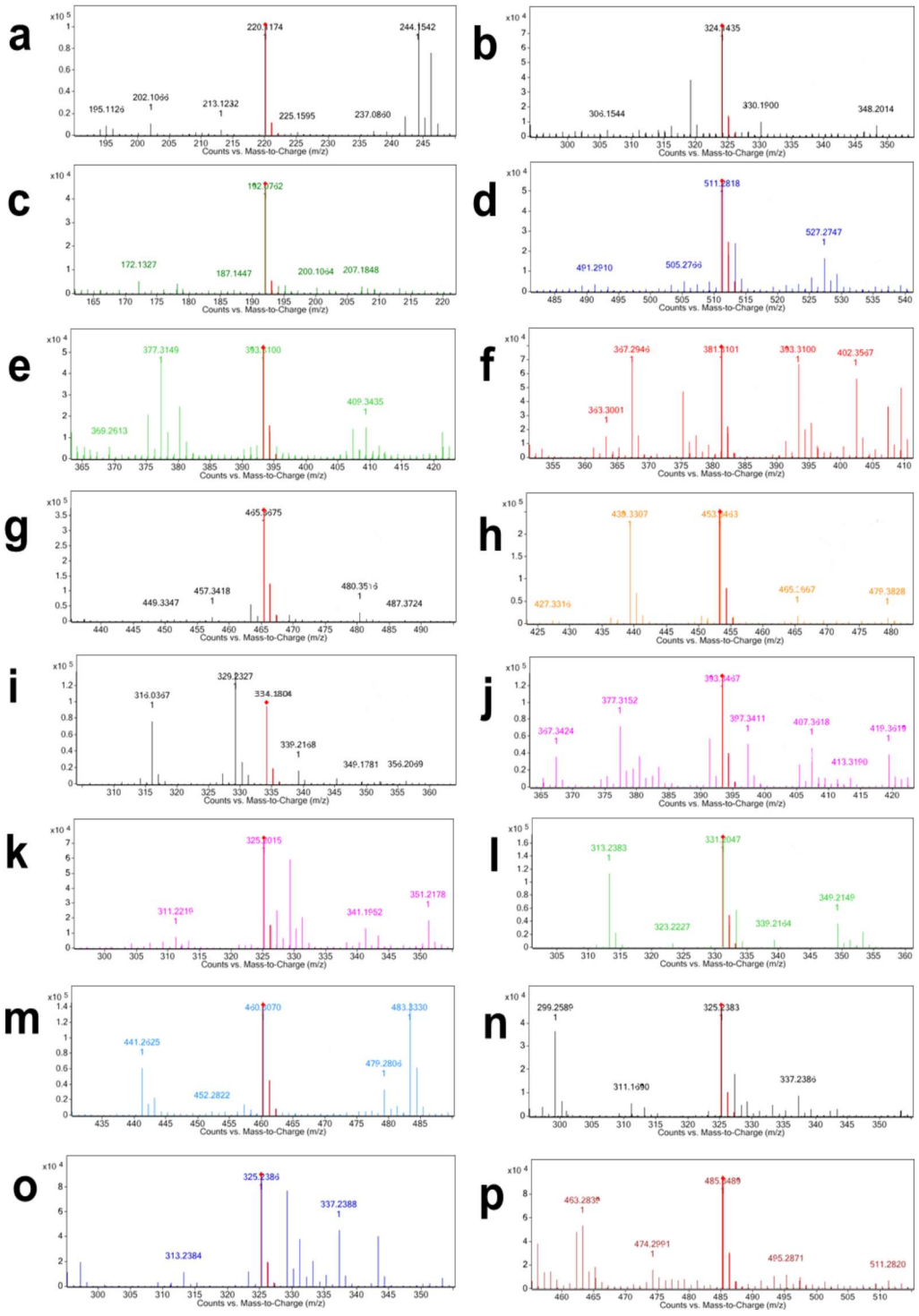
a
220.1174
244.1542
195.1126
202.1066
213.1232
225.1595
237.0860
b
324.1435
306.1544
330.1900
348.2014
c
192.1762
172.1327
187.1447
200.1064
207.1848
d
511.2818
527.2747
491.2910
505.2766
e
377.3149
393.3100
409.3435
369.2613
f
367.2946
381.3101
393.3100
402.3567
363.3001
g
465.3675
457.3418
480.3516
449.3347
487.3724
h
439.3307
453.3443
465.3667
479.3828
427.3316
i
329.2327
316.0367
334.1804
339.2168
349.1781
356.2069
j
393.3447
377.3152
397.3411
407.3618
419.3615
367.3424
413.3190
k
325.2015
311.2219
341.1952
351.2178
l
313.2383
331.2047
349.2149
323.2227
339.2164
m
460.3070
483.3330
441.2625
479.2806
452.2822
n
299.2589
325.2383
311.1690
337.2386
o
325.2384
337.2388
313.2384
p
485.3489
463.2838
474.2991
495.2871
511.2820

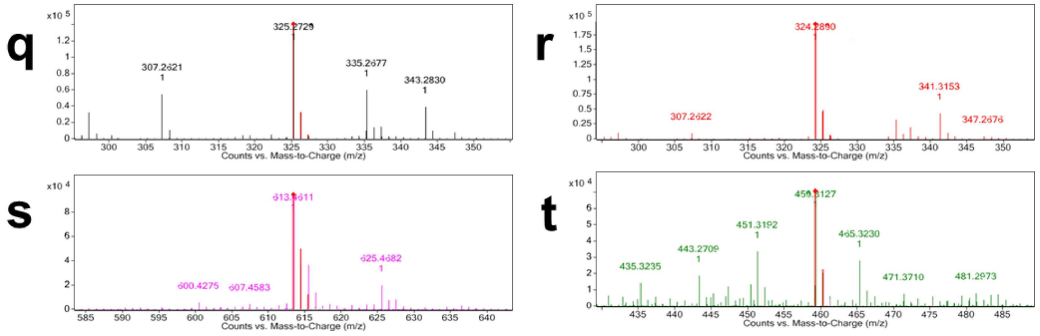

Figure 3.9. MS spectra of (a) D- pantothenic acid (b) acremoauxin A (c) carbendazim (d) cephaeline (e) asterosterol (f) ophiobolin F (g) betulin (h) 16,28-Secosolanidan-23-ol,3-amino-16,23-epoxy-, (3beta,5alpha,16alpha,22alpha,23beta,25beta)- (i) Senecionine (j) Cholest-5-ene (k) (3b,6b,8a,12a)-8,12-epoxy-7(11)-eremophilene-6,8,12-trimethoxy-3-ol (l) beta-obscurine (m) myxalamid B (n) avocadyne 1-acetate (o) avocadyne 4-acetate (p) momordol (q) (13R,14R)-7-Labdene-13,14,15-triol (r) linoleoyl ethanolamide (s) dihydroanhydorhodovibrine and (t) polyporusterone G.

Table 3.3. LC-QTOF/MS- based tentative identified of myco-metabolites in PO1, HFPO1, and EFPO1 of *P. osteratus*.

No.	RT	Molecular ion, m/z	Mass	Adduct ion	Elemental composition	Myco-metabolite identification	Class of myco-metabolite	Relative abundance		
								PO1	HFPO1	EFPO1
1	4.147	220.1174	219.1102	$(M+H)^+$	C9 H17 N O5	D- pantothenic acid (PAN)	Fatty acid	++	-	-
2	6.609	324.1435	323.1365	$(M+H)^+$	C16 H21 N O6	Acremoauxin A (ACR)	Indole alkaloid	-	-	+
3	6.897	192.0762	191.069	$(M+H)^+$	C9 H9 N3 O2	Carbendazim (CAR)	Trytophan alkaloid	++		+
4	8.743	511.2818	466.2815	$(M+HCOO)^-$	C28 H38 N2 O4	Cephaeline (CEP)	Isoquinoline alkaloid	-	-	+
5	8.969	393.3100	370.3213	$(M+Na)^+$	C26 H42 O	Asterosterol (AST)	Steroids	-	++	+
6	9.19	381.3101	358.3211	$(M+Na)^+$	C25 H42 O	Ophiobolin F (OPH)	Sesterterpenoid	+	++	-
7	10.165	465.3675	442.3783	$(M+Na)^+$	C30 H50 O2	Betulin (BET)	Triterpenoid	++	+++	+
8	10.631	453.3463	430.3570	$(M+Na)^+$	C27 H46 N2 O2	16,28-Secosolanidan-23-ol,3-amino-16,23-epoxy-, (3beta,5alpha,16alpha,22alpha ,23beta,25beta)- (SOL)	Steroidal alkaloid	++	+++	+
9	10.713	334.1654	335.1727	$(M-H)^-$	C18 H25 N O5	Senecionine (SEN)	Pyrrolizidine alkaloid	+	-	++
10	10.771	393.3467	370.3573	$(M+Na)^+$	C27 H46	Cholest-5-ene (CHOL)	Steroids	++	+++	+
11	12.127	325.2015	326.2087	$(M-H)^-$	C18 H30 O5	(3b,6b,8a,12a)-8,12-epoxy-7(11)-eremophilene-6,8,12-trimethoxy-3-ol (ERE)	Sesquiterpenoid	-	+	-
12	15.921	331.2047	272.1888	$(M+CH3COO)^-$	C17 H24 N2 O	Beta-obscurine (OBS)	Pyridine alkaloid	-	+++	-
13	16.008	460.307	401.293	$(M+CH3COO)^-$	C25 H39 N O3	Myxalamid B (MYX)	Linear polyketides	-	+++	-
14	16.582	325.2383	326.2456	$(M-H)^-$	C19 H34 O4	Avocadyne 1-acetate (AVO1)	Fatty alcohol	-	-	+
15	16.602	325.2386	326.2459	$(M-H)^-$	C19 H34 O4	Avocadyne 4-acetate (AVO4)	Fatty alcohol	-	++	-
16	16.888	485.3489	440.3506	$(M+HCOO)^-$	C26 H48 O5	Momordol (MOM)	Linear polyketides	-	++	-
17	17.366	325.2729	324.2656	$(M+H)^+$	C20 H36 O3	(13R,14R)-7-Labdene-13,14,15-triol (LAB)	Diterpenoid	++	+++	-
18	17.674	324.289	323.2815	$(M+H)^+$	C20 H37 N O2	Linoleoyl ethanolamide (LIN)	Fatty alcohol	++	+++	+
19	18.595	613.4611	568.4612	$(M+HCOO)^-$	C41 H60 O	Dihydroanhydorhodovibrine (RHOD)	Carotenoid	+	-	-
20	18.782	459.3127	460.3199	$(M-H)^-$	C28 H44 O5	Polyporusterone G (POL)	Steroids	-	+	-

3.4.5. Chemometric analysis

An unsupervised, descriptive model: PCA and HCA were adopted to analyze metabolite variability between the samples. PCA remains the workhorse and works as a gold standard model among all the unsupervised chemometric methods. It is a projection-based method and a mathematically rigorous process that provide a qualitative visual representation of similarity and dissimilarity between and within the sample (Tugizimana et al., 2013).

The established model resulted in the R2X(cum) 1 (R2X(1) 0.703 and R2X(2) 0.297) and Q2(cum) 0.99. As the R2X (cum) value is close to 1, the Q2(cum) value is > 0.5, thus suggesting the established PCA model is a good model with good predictivity. The PCA biplot (Figure 3.10.a) showed that myco-metabolite like cephaline (CEP), acremoauxin A (ACR), avocadyne 1-acetate (AVO1), and senecionine (SEN) forms a closer angle < 90˚ with EFPO1, thus they were closely correlated to EFPO1. Similarly, myco-metabolites (betulin (BET), 16,28-Secosolanidan-23-ol,3-amino-16,23-epoxy-, (3beta,5alpha,16alpha,22alpha,23beta,25beta)- (SOL), asterosterol (AST), (3b,6b,8a,12a)-8,12-epoxy-7(11)-eremophilene-6,8,12-trimethoxy-3-ol (ERE), beta-obscurine (OBS), myxalamid B (MYX), momordol (MOM), avocadyne 4-acetate (AVO), ophiobolin F (OPH), linoleoyl ethanolamide (LIN), (13R,14R)-7-Labdene-13,14,15-triol (LAB), and cholest-5-ene (CHOL),) were closely related to HFPO1 fraction, making an angle < 90˚ with HFPO1. On the other hand, fraction HFPO1 and EFPO1 were negatively correlated, as they diverge and form a large angle (close to 180˚). In the same way, myco-metabolites closely correlated to EFPO1 and those closely correlated to HFPO1 were situated on extreme left and right, thus diverging and making larger angles as shown in loading plot (Figure 3.10.b). The HCA-driven

dendrogram, another unsupervised model, portrays a graphical representation of metabolic variability between the given sample. HCA clusters the data in the distance to reflect the dissimilarities between the sample. The dendrogram (Figure 3.10.c) includes three main clusters or groups; Group 1 (green), encompasses all the myco-metabolites closely related to PO1, Group 2 (blue), with all the myco-metabolites closely associated with EFPO1, and Group 3 (red) highlighting myco-metabolites closely engaged with HFPO1. The resultant HCA was in alignment with the PCA result, wherein, Group 2 and Group 3 were distant apart, thus further validating the PCA finding.

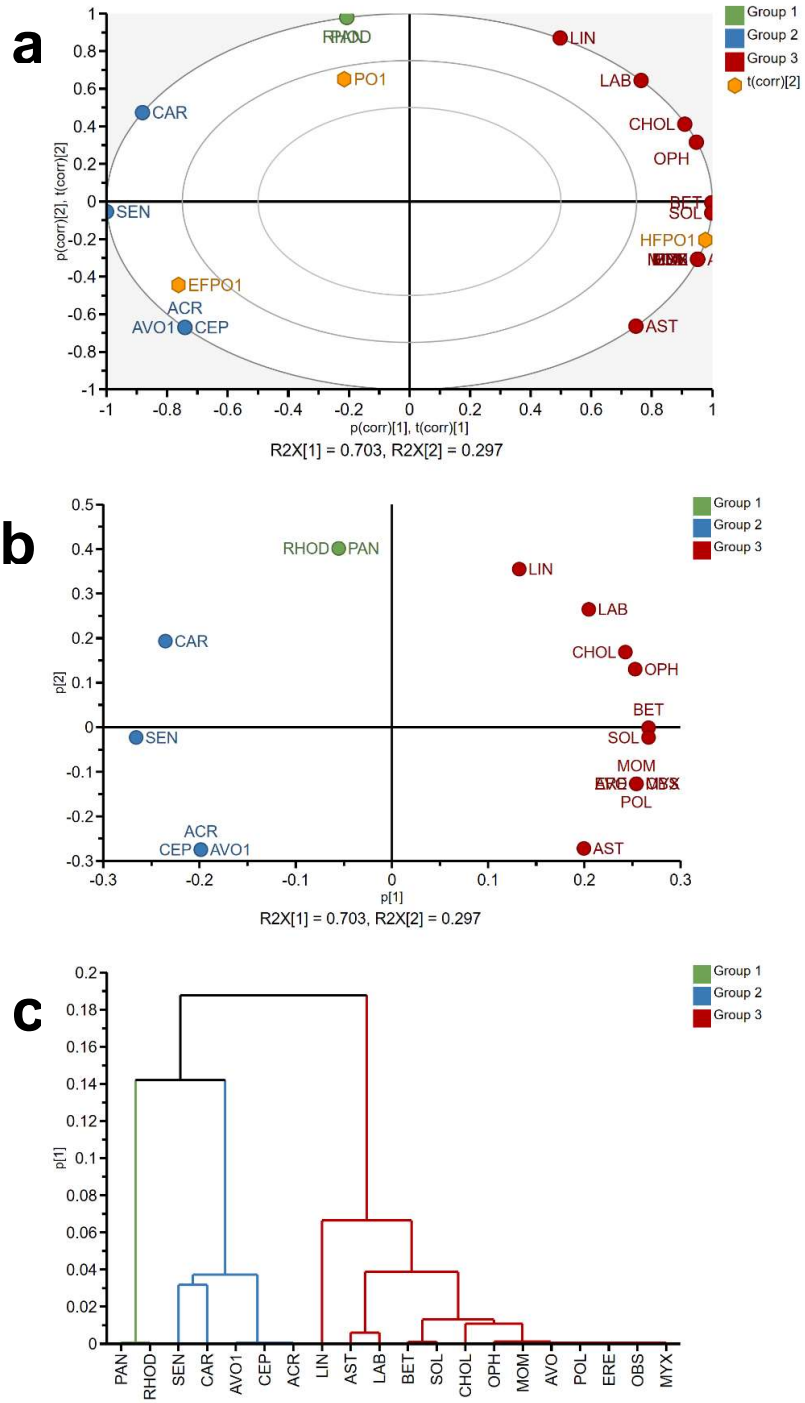

Figure 3.10. Unsupervised chemometric analysis of PO1, HFPO1, and EFPO1 (a) Bi-plot of PCA analysis of identified myco-metabolites in PO1, HFPO1, and EFPO1; (b) Loading plot of PCA analysis of the identified myco-metabolites in PO1, HFPO1, and EFPO1; and (c) HCA dendrogram of identified myco-metabolites in PO1, HFPO1, and EFPO1.

PLS, a supervised predictive model, was assessed to correlate the bioactivities of the given sample with myco-metabolites. The model was validated using 100 random permutations, and the resultant R2 and Q2 were close to 1, thus suggesting an established PLS model, a good model with good predictive power. A 3-D view of the loading plot was shown in (Figure 3.11.a.), where bioactivities against a major panel of cancer cell lines (except A549, SSC9, and MiaPaCa-2) were closely associated with metabolites (betulin, 16,28-Secosolanidan-23-ol,3-amino-16,23-epoxy-, (3beta,5alpha,16alpha,22alpha,23beta,25beta)-, ophiobolin F, linoleoyl ethanolamide, (13R,14R)-7-Labdene-13,14,15-triol, asterosterol, cholest-5-ene, (3b,6b,8a,12a)-8,12-epoxy-7(11)-eremophilene-6,8,12-trimethoxy-3-ol, beta-obscurine, myxalamid B, momordol, avocadyne 4-acetate). As per PLS- biplot (Figure 3.11.b.), the myco-metabolite contributing to bioactivities were closely associated with the HFPO1. VIP score of metabolites contributing to bioactivities were more than 0.5, indicating the significance of metabolites in bioactivities (Figure 3.11.c.).

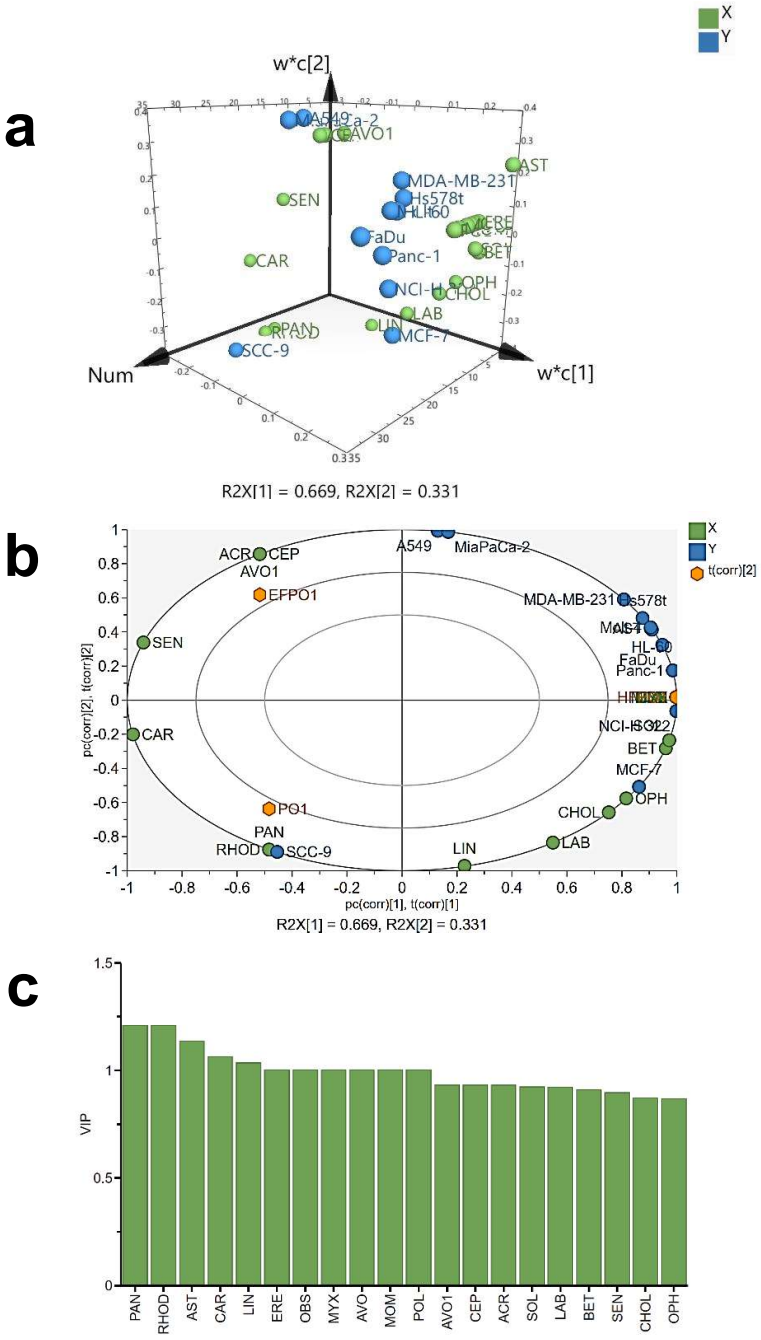

Figure 3.11. Supervised chemometric analysis of PO1, HFPO1, and EFPO1 (a) 3-D view of loading plot of PLS analysis of identified myco-metabolites contributing to bioactivities, in PO1, HFPO1, and EFPO1; (b) Bi-plot of PLS analysis of the identified myco-metabolites contributing to bioactivities, in PO1, HFPO1, and EFPO1; and (c) VIP score of the identified myco-metabolites contributing to bioactivities, in PO1, HFPO1, and EFPO1.

3.4.6. Headspace Gas Chromatography (GC-HS) based solvent residual analysis

The residual hexane and ethyl acetate solvent in HFPO1, and EFPO1 were below the detection limit. The solvent analysis reports of HFPO1, AND EFPO1, are attached in *Appendix* (Figure A3, and Figure A4, respectively).

3.5. Summary

On the ground of *in-vitro* cytotoxic activity from preliminary studies, DCM: Et crude extract of *P. osteratus* (PO1) was preferred for further exploration, and bio-assay guided fractionation of PO1 was performed. The cytotoxic potential of HFPO1 and EFPO1 fractions were significantly strong against MDA-MB-231, and A549 as compared to BFPO1 and AFPO1 fractions of PO1. Based on the literature outlook, polyphenol and ergosterol were the main lower molecular weight entities responsible for anti-cancer potential. Based on this, LC-MS/MS polyphenol and ergosterol-based profiling and quantification of PO1, HFPO1, and EFPO1 were performed. Despite being significantly rich in polyphenol and ergosterol, EFPO1 fraction bioactivities against major of studied cancer cell lines were moderate. Reciprocally, HFPO1 fraction containing a significantly low amount of polyphenols and ergosterol, showed higher cytotoxic potential. This finding indicated the role of the alternative entities responsible for observed bioactivities.

With this aim, untargeted LC-QTOF/MS myco-metabolites profiling of PO1, HFPO1, and EFPO1 was executed at full scan positive and negative mode. About 20 myco-metabolites were scrutinized. Of 20 myco-metabolite identified, HFPO1 fraction showed the appreciable abundances of cholestane steroids, terpenoid (sesterterpenoid, diterpenoid, sesquiterpenoid, and triterpenoid), fatty alcohol, polyketides, steroidal alkaloid. A moderate abundance of alkaloids, steroids, terpenoid, fatty alcohol were present in PO1. On the other hand, appreciable abundances of alkaloids, with low to

negligible abundance of terpenoid, fatty alcohol, and steroids, were present in the EFPO1 fraction.

Collectively, PO1 was an amalgamation of metabolites such as alkaloids, steroids, terpenoids, fatty alcohol, and carotenoids. From the crude extract, HFPO1 fraction preferentially extracts steroids, terpenoid, and a fatty alcohol class of metabolite. While, polyphenol, ergosterol, and alkaloids were primarily extracted in EFPO1 fraction. This differential extraction of myco-metabolites were responsible for the observed variable bioactivities of the studied extract and fraction.

As per PCA analysis, metabolites with high abundance in HFPO1 and EFPO1 were on the opposite side of each other, making them negatively correlated. A similar result was in the alignment of HCA analysis, where both the groups of HFPO1 and EFPO1 were distant apart. The bi-plot of PLS studies showed the higher abundance of metabolites of HFPO1 fraction that could be responsible for its higher cytotoxic activity against major cancer cell lines. The possible myco-metabolites contributing to bioactivities of HFPO1 were betulin, solanocapsine, ophiobolin F, linoleoyl ethanolamide, (13R,14R)-7-labdene-13,14,15-triol, asterosterol, cholest-5-ene, (3b,6b,8a,12a)-8,12-epoxy-7(11)-eremophilene-6,8,12-trimethoxy-3-ol, beta-obscurine, myxalamid B, momordol, avocadyne 4-acetate, belonging to the class of steroid, terpenoids, steroidal alkaloids, fatty alcohol, and polyketides.